A gradient viscosity model for estimating CO2 permeability of amino acid ionic liquid-based facilitated transport membrane

Matsuoka, Atsushi
Otani, Akihito
Kamio, Eiji
Matsuyama, Hideto

(Citation)
Separation and Purification Technology,280:119847

(Issue Date)
2022-01-01

(Resource Type)
journal article

(Version)
Accepted Manuscript

(URL)
https://hdl.handle.net/20.500.14094/90009127

A gradient viscosity model for estimating CO_2 permeability of amino acid ionic liquid-based facilitated transport membrane

Atsushi Matsuoka, Akihito Otani, Eiji Kamio, and Hideto Matsuyama[*]

Research Center for Membrane and Film Technology, Department of Chemical Science and Engineering, Kobe University, 1-1 Rokkodai, Nada, Kobe 657-8501, Japan

Corresponding author

Email: matuyama@kobe-u.ac.jp

ABSTRACT. Amino acid ionic liquids (AAILs) are used as a CO_2 carrier in facilitated transport membranes (FTM) due to their high CO_2 permselectivity. However, estimating the membrane performance of these FTMs is difficult because the viscosity of the AAIL increases with the CO_2 absorption. Therefore, potential models were investigated to accurately estimate the CO_2 permeability of an AAIL-based FTM. Herein, models were constructed to estimate the CO_2 absorption amount and viscosity of the AAIL through simulations at various CO_2 partial pressures

and temperatures. Furthermore, the CO_2 permeability of the AAIL-based FTM at various conditions were estimated based on the models and compared to the experimental data. Consequently, we reported a model that expressed the viscosity gradient of the AAIL in the FTM by dividing the membrane into small intervals to estimate the CO_2 permeability with high accuracy.

KEYWORDS: CO_2 separation membrane, facilitated transport membrane, gas permeation mechanism, ionic liquid carrier

1. INTRODUCTION

The development of an efficient CO_2 separation technique is essential to overcome global climate change. Membrane separation processes have been reported to be a less energy-intensive alternative compared to other separation techniques.[1–3] Although the large number of polymer-based membranes were investigated, the CO_2 separation performance of the polymer membranes were limited by an upper bound.[4] Therefore, the development of innovative types of membranes with high CO_2 permselectivity is essential to improve the efficiency of the membrane process. A facilitated transport membrane (FTM) containing a carrier was investigated to overcome the limitations of the polymer membranes.[5–13] The carrier in the FTMs selectively reacts with CO_2 enabling high CO_2 permselectivity. Conventionally, aqueous amine solutions were widely investigated as the carrier of the FTMs.[14–18] The FTMs with the amine solution demonstrated excellent CO_2 permselectivity at low CO_2 partial pressure and high humidity. However, at low humidity, this FTM displayed low CO_2 permselectivity because of the need of water for the diffusion of the solutes and the reaction between amine and CO_2.[6,19]

Recent research has reported that an amino acid ionic liquid (AAIL) could act as a CO_2 carrier of FTMs. Kasahara *et al*. first reported an AAIL-based supported ionic liquid membranes (SILM) for CO_2 separation demonstrating high CO_2 permselectivity even in dry conditions.[20] The design of the chemical structure of the cation and anion of the AAIL carrier in the FTMs could control CO_2 permselectivity.[21,22] However, the AAIL-based SILMs were hard to be used under pressurized condition because the AAIL were held in the porous support with the weak capillary force. Consequently, Moghadam *et al.* developed an AAIL-based tough ion gel membrane to overcome this problem. The prepared ion gel membranes demonstrated excellent toughness and pressure resistance as well as high CO_2 permselectivity.[23–25]

Therefore, the membrane separation process with the AAIL-based FTM is a promising candidate for effective CO_2 separation. The practical use of AAIL-based FTMs necessitates the fabrication of a membrane module to reduce the installation volume. In the membrane module, the composition of the feed-side gas would be different at every position of the module. Therefore, to optimize the design of the membrane module constructed using AAIL-based FTMs, the CO_2 permeance of the FTM at various gas compositions should be evaluated.

To establish the model for estimating the CO_2 permeability of the AAIL-based FTMs, the viscosity change of the AAIL with CO_2 absorption should be considered because the diffusivity of the solute strongly affected by the viscosity of the solvent. Even in the gel materials, the diffusion coefficient of the solutes would depends on the viscosity of the solvent.[26] Thus, the viscosity of the AAIL is crucial to consider the CO_2 permeability of the AAIL-based FTMs.

It was reported that the viscosity increase of the AAIL was caused by the formation of the hydrogen bonding network between the CO_2-AAIL complexes (carbamic acid and carbamate) that produced by the reaction between the AAIL and CO_2.[27–30] Therefore, the higher concentration of the CO_2-AAIL complex results in a higher viscosity of the AAIL. In the AAIL-based FTM, the concentration of the CO_2-AAIL complexes gradually decreases from the feed side surface to the permeate side surface as a result of the diffusion of the complex through the FTMs. Consequently, this concentration gradient of the CO_2-AAIL complexes leads to different viscosities of the AAIL at each position in the FTM. Since the viscosity of the AAIL strongly affects the diffusivity of the solutes in the AAIL-based FTM,[31–33] the solutes would demonstrate different diffusivities at each position in the membrane.

There have been some reports on models to estimate the CO_2 permeability for the conventional FTMs that use an amine solution.[34–37] However, the majority of these models did

not consider the effect of the viscosity change caused by the CO_2 absorption. To consider the effect of the viscosity gradient in the AAIL-based FTMs on the CO_2 permeability, Kasahara et al. adopted the mean viscosity model that used the average viscosity of the AAIL at the feed and permeate sides (see 3.3.1 for detail).[38] However, especially at low temperatures, the mean viscosity model cannot explain the experimental data. Therefore, the conventional models could not accurately express the effect of the viscosity gradient of the AAIL that influences the CO_2 permeability. Thus, it is imperative to develop a new calculation model that considers the viscosity gradient to estimate the CO_2 permeability in FTMs. Herein, we present a new highly accurate model to estimate the CO_2 permeability that considers the continuous change in the diffusion coefficients at various positions in the FTM.

2. EXPERIMENTAL SECTION

2.1 Materials

All reagents were used as received. Tetrabutylphosphonium hydroxide ($[P_{4444}][OH]$) 40 wt% in H_2O was purchased from Sigma-Aldrich Co. (St. Louis, MO, USA) and used as the cation source of the AAIL. L-glycine (99.8 %) was purchased from Tokyo Chemical Industry Co. (Tokyo, Japan) and used as the anion source of the AAIL. Acetonitrile (99.9 %) and methanol (99.8 %) used for the purification of the AAIL were purchased from Sigma-Aldrich Co. and Wako Pure Chemicals Industry Ltd. (Osaka, Japan), respectively.

2.2 Synthesis of IL

In this study, tetrabutylphosphonium glycinate ([P_{4444}][Gly]) was used as an AAIL. The AAIL was synthesized through a neutralization reaction between [P_{4444}][OH] and L-glycine. The details of the synthesis scheme are described in the Supporting Information.

2.3 Viscosity measurement

The viscosity of the AAIL was measured using an Electro-Magnetically Spinning Sphere Viscometer (EMS-1000W, Kyoto Electronics Manufacturing Co.) with a metallic sphere rotating at a speed of 1000 rpm. The CO_2 partial pressure in the sample tube was controlled by bubbling CO_2/N_2 mixed gas into the AAIL. The flow rates of CO_2 and N_2 gases were controlled using a mass flow controller (Hemmi Slide Rule Co. Ltd., Japan), calibrated by a soap-film flow meter (HORIBA STEC Ltd., Japan). The viscosity of the AAIL was continuously measured to confirm that the CO_2 absorption to the AAIL was reached equilibrium. (supporting information) The viscosities of the AAIL were measured between 303 K and 373 K.

2.4 Gas permeation experiments

The gas permeation experiments were conducted using a SILM. A hydrophilic PTFE microporous support membrane with a thickness of 35 μm and pore size of 100 nm, was purchased from Toyo Roshi Kaisha, Ltd., Japan. This support membrane was immersed into the synthesized [P_{4444}][Gly], and degassed for 30 min to fill the pores of the PTFE membrane with [P_{4444}][Gly]. The [P_{4444}][Gly]-impregnated PTFE membrane was retrieved from [P_{4444}][Gly], and the excess [P_{4444}][Gly] on the membrane surface was wiped off.

The experimental setup for the gas permeation test is illustrated in Figure S1 in the Supporting Information. The supported [P_{4444}][Gly] membrane was set on a flat permeation cell

made of stainless steel. The effective membrane area of the cell was 2.88 cm^2. The cell was placed in a thermostat oven to maintain a constant temperature. The feed gas was prepared by mixing CO_2 and N_2. The flow rates of these gases were controlled by a mass flow controller (Hemmi Slide Rule Co. Ltd., Japan), calibrated by a soap-film flow meter (HORIBA STEC Ltd., Japan). The total flow rate and total pressure of the feed gas was maintained at 8.18×10^{-3} mol s^{-1} and atmospheric pressure, respectively. The partial pressures of CO_2 and N_2 in the feed gas were controlled by the flow rates of CO_2 and N_2. On the other hand, helium was used as the sweep gas on the permeate side. The flow rate of helium was set at 1.64×10^{-3} mol s^{-1} using a calibrated mass flow controller. The total pressure on the permeate side was maintained at atmospheric pressure. The CO_2 and N_2 that permeated through the membrane were swept using helium, and the composition of the sweep gas was measured using a gas chromatograph (GC-8A, Shimadzu Co., Japan). The amounts of CO_2 and N_2 that permeated through the membrane were determined from the concentrations of the gases and the flow rate of the sweep gas. Each experiment was continued until the difference in the peak areas of the gases measured by GC was less than 1%.

3. RESULTS AND DISCUSSION

3.1 Estimation of the amount of CO_2 absorbed in the AAIL

In an AAIL-based FTM, the AAIL carrier act as the mobile CO_2 carrier. Therefore, the CO_2 permeated through the membrane by the facilitated transport mechanism with the mobile carrier. the CO_2 permeates through the membrane *via* a series of the elementary processes including: (1) complex formation reaction at the feed side membrane surface, (2) diffusion of CO_2-AAIL complex across the membrane, and (3) the decomposition of the complex at the permeate side of the membrane surface. The high viscosity of the AAIL indicates that the diffusion process

would be the rate determining step of the CO_2 permeation through the AAIL-based FTM.[38] Therefore, the CO_2 permeability of the AAIL-based FTM was estimated considering only the diffusion rate. CO_2 diffuses through the membrane in two forms, a physically absorbed CO_2 and CO_2-AAIL complexes formed by the absorption reaction. Kasahara et al. previously reported the theoretical analysis of the CO_2 absorption isotherms of the AAIL.[38] In their analysis, the following equations were assumed.

$$CO_2(gas) \leftrightarrow CO_2(AAIL), \quad (1)$$

$$CO_2(AAIL) + R–NH_2 \leftrightarrow R–N^+H_2COO^-, \quad (2)$$

$$R–N^+H_2COO^- + R–NH_2 \leftrightarrow R–NHCOO^-\ldots N^+H_3 –R, \quad (3)$$

However, some reasurchers reported that the $R–NHCOO^-$ and $R–NH_3^+$ were formed after the second reaction. (eq. 3) [27–30] Goodrich *et al.* reported the CO_2 absorption process of the AAIL being composed of reactions forming carbamic acid and carbamate, as depicted in the following equations.[27]

$$CO_2(gas) \leftrightarrow CO_2(AAIL), \quad (4)$$

$$CO_2(AAIL) + R–NH_2 \leftrightarrow R–N^+H_2COO^- (com1), \quad (5)$$

$$R–N^+H_2COO^- + R–NH_2 \leftrightarrow R–NHCOO^- (com2) + R–NH_3^+, \quad (6)$$

where, $CO_2(gas)$ and $CO_2(AAIL)$ represent the CO_2 molecule in the gas phase and the CO_2 molecule dissolved in the AAIL, respectively. $R–NH_2$, $R–NH_3^+$, $R–N^+H_2COO^-$, and $R–NHCOO^-$ are anions of the AAIL, a protonated anion of AAIL, a carbamic acid, and a carbamate, respectively. The counter cation of the AAIL was excluded from these equations. Hereafter, $R–N^+H_2COO^-$ and $R–NHCOO^-$ are referred as com1 and com2, respectively. These equations indicate that facilitated CO_2 permeation was occurred by the transport of com1 and com2. On the other hand, CO_2 permetion based on the solution-diffusion mechanism was occured by the transport of

CO_2(AAIL). Therefore, the CO_2 permeability was estimated by considering the diffusion fluxes of these three components: physically absorbed CO_2, com1, and com2. The total CO_2 flux can be expressed through the summation of these diffusion fluxes using the following equation.

$$J_{CO2} = \sum_{i} D_i \left(\frac{dC_i}{dz}\right), \quad (7)$$

where i represents the physically absorbed CO_2, com1, or com2. J_{CO2} [mol m^{-2} s^{-1}] is the total CO_2 flux through the membrane, z [m] is the position in the membrane, D_i [m^2 s^{-1}] is the diffusion coefficient of the component i in the AAIL, and C_i [mol m^{-3}] is the concentration of the component i at position z. To estimate the CO_2 permeability of the AAIL-based FTM, it is necessary to simulate the concentration of solutes and the diffusion coefficient of solutes in the AAIL at various CO_2 partial pressures and temperatures. In this section, an equation that can simulate the CO_2 absorption amount in the AAIL at various CO_2 partial pressures and temperatures was investigated.

The theoretical analysis of the CO_2 absorption by the AAIL was conducted based on the model reported by Goodrich *et al.*[27] The following equation was obtained using the Henry's law constant and the equilibrium constants for each reaction.

$$H_{CO_2} = \frac{C_{CO_2}}{p_{CO_2}}, \quad (8)$$

$$K_{com1} = \frac{C_{com1}}{C_{AAIL} C_{CO_2}}, \quad (9)$$

$$K_{com2} = \frac{C_{com2} C_{R-NH3+}}{C_{AAIL} C_{com1}}, \quad (10)$$

where H_{CO2} [mol m^{-3} kPa^{-1}] is the Henry's law constant for CO_2 absorption into the AAIL. p_{CO2} [kPa] is the CO_2 partial pressure. K_{com1} [mol^{-1} m^3] and K_{com2} [-] are the equilibrium constants of the reactions presented in Eqs. 5 and 6, respectively. On the other hand, the mass balance of the AAIL is expressed as follows,

$$C_{\mathrm{AAIL,int}} = C_{\mathrm{AAIL}} + C_{\mathrm{com1}} + C_{\mathrm{com2}} + C_{\mathrm{R-NH3+}}, \quad (11)$$

$$C_{\mathrm{com2}} = C_{\mathrm{R-NH3+}}, \quad (12)$$

where, $C_{\mathrm{AAIL,int}}$ [mol m^{-3}] is the concentration of AAIL in the initial state. The total amount of CO_2 absorbed in the AAIL, $C_{\mathrm{CO2,total}}$ [mol m^{-3}] can be derived from Eqs 8–12, and is expressed through the following equations,

$$C_{\mathrm{CO_2,total}} = p_{\mathrm{CO_2}} H_{\mathrm{CO_2}} + \frac{p_{\mathrm{CO_2}} H_{\mathrm{CO_2}} K_{\mathrm{com1}} C_{\mathrm{AAIL,int}}}{(1 + p_{\mathrm{CO_2}} H_{\mathrm{CO_2}} K_{\mathrm{com1}} + 2\beta)} + \frac{\beta C_{\mathrm{AAIL,int}}}{(1 + p_{\mathrm{CO_2}} H_{\mathrm{CO_2}} K_{\mathrm{com1}} + 2\beta)}$$
$$\beta = \sqrt{K_{\mathrm{com1}} K_{\mathrm{com2}} p_{\mathrm{CO_2}} H_{\mathrm{CO_2}}} \quad (13)$$

From Eq. 13, the relationship between the total CO_2 absorption amount at a particular temperature and CO_2 partial pressure was calculated using H_{CO2}, K_{com1} and K_{com2} as the fitting parameters. These fitting parameters were determined by fitting the calculated relationship between the total CO_2 absorption amount and CO_2 partial pressure to the experimental results. Herein, we used the experimental results of the CO_2 absorption isotherms of the AAIL reported by Kasahara *et al*.[38] Figure 1(a) displays the results of the fitting at various temperatures. The equilibrium constants obtained using the fittings are listed in Table 1. As illustrated in Figure 1(a), the calculated CO_2 absorption isotherms are consistent with the experimental results at all temperatures. This result suggests that Eq. 13 appropriately estimates the CO_2 absorption amount of the AAIL. Therefore, the equilibrium concentration of physically absorbed CO_2, com1, and com2 at various CO_2 partial pressures could be calculated by using Eqs. 8–13.

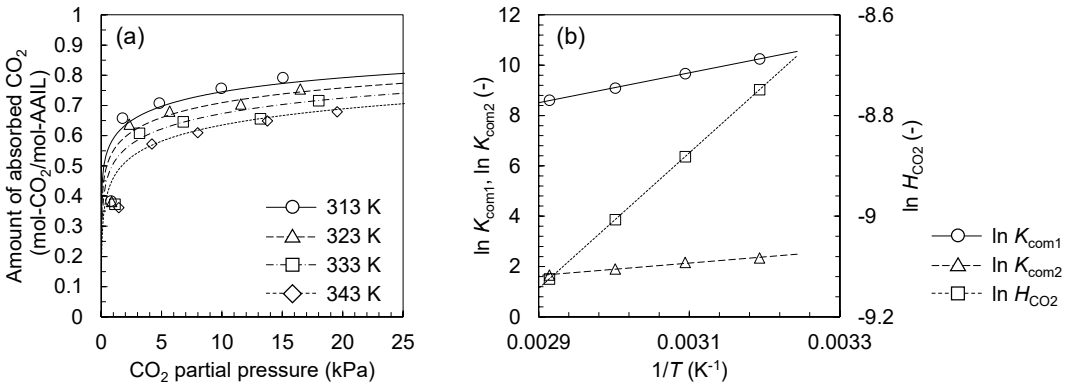

Figure 1 (a) CO_2 absorption isotherms of [P_{4444}][Gly] at various temperatures. The plots indicate the experimental results reported in Ref [38] and the lines represent the results calculated using Eq. (13). (b) van't Hoff plots of the Henry's law constant for CO_2 absorption in [P_{4444}][Gly] and the equilibrium constants of the carbamic acid and carbamate forming reactions for [P_{4444}][Gly].

Table 1 Henry's law constants of the CO_2 absorption in the [P_{4444}][Gly] and equilibrium constants of the reactions of Eqs. 5 and 6 at various temperatures determined through the fittings.

Temperature [K]	H_{CO2} [mol m^{-3} kPa^{-1}]	K_{com1} [mol^{-1} m^3]	K_{com2} [-]
313.15	1.59×10^{-4}	2.84×10^{4}	10.4
323.15	1.39×10^{-4}	1.58×10^{4}	8.72
333.15	1.23×10^{-4}	8.87×10^{3}	6.72
343.15	1.09×10^{-4}	5.48×10^{3}	5.26

The equilibrium constants at various temperatures were determined to calculate the concentration of each solute at that temperature. The temperature dependence of the Henry's law constant, H_{CO2}, and the equilibrium constants of the reactions, K_{com1} and K_{com2}, can be expressed using the following van't Hoff equations.

$$\ln H_{CO_2} = -\frac{\Delta H_{CO_2}}{RT} + \frac{\Delta S_{CO_2}}{R}, \quad (14)$$

$$\ln K_{comi} = \frac{\Delta H_{comi}}{RT} + \frac{\Delta S_{comi}}{R}, i = 1, 2, \quad (15)$$

where, ΔH_{CO2} [J mol^{-1}] and ΔS_{CO2} [J mol^{-1} K^{-1}] are the mole enthalpy change and the mole entropy change of the physical absorption of CO_2 into the AAIL. ΔH_{comi} [J mol^{-1}] and ΔS_{comi} [J mol^{-1} K^{-1}] are the enthalpy change and entropy change of the reactions. R [J mol^{-1} K^{-1}] is the gas constant, and T [K] represents the temperature. The van't Hoff plots based on Eqs. 14 and 15 for each equilibrium constant illustrated in Figure 1(b). The mole enthalpy changes (ΔH_{CO2}, ΔH_{com1}, ΔH_{com2}) and the mole entropy changes (ΔS_{CO2}, ΔS_{com1}, ΔS_{com2}) listed in Table 2 were determined using the slope and intercept of each plot, respectively. Consequently, the equilibrium constants at various temperatures were calculated from the enthalpy and entropy changes displayed in Table 2 using the Eqs. 14 and 15. Thus, the concentration of each solute at various temperatures and CO_2 partial pressures could be estimated.

Table 2 Thermodynamic constants for CO_2 absorption by [P_{4444}][Gly].

Physical absorption		com1 formation		com2 formation	
ΔH_{CO2}	ΔS_{CO2}	ΔH_{com1}	ΔS_{com1}	ΔH_{com2}	ΔS_{com2}
[kJ mol^{-1}]	[J mol^{-1} K^{-1}]	[kJ mol^{-1}]	[J mol^{-1} K^{-1}]	[kJ mol^{-1}]	[J mol^{-1} K^{-1}]
−11.2	−108.5	−49.3	−72.2	−20.6	−45.9

3.2 Estimation of the viscosity of the AAIL

The diffusion coefficients of the component i in the AAIL were determined from the viscosity of the AAIL using the Wilke-Chang equation displayed in the following Eq. 16.[31,33]

$$D_{\mathrm{i}} = 7.4 \times 10^{-12} \frac{\sqrt{\psi_{\mathrm{AAIL}} M_{\mathrm{AAIL}}}}{\eta_{\mathrm{AAIL}} V_{\mathrm{i}}^{0.6}} T, \qquad (16)$$

where ψ_{AAIL} [-], M_{AAIL} [g mol^{-1}], and η_{AAIL} [mPa s] are the association constant, molecular weight and the viscosity of the AAIL, respectively. V_{i} [m^3 mol^{-1}] is the molar volume of the component i. This equation suggests that the viscosity of the AAIL at various CO_2 partial pressures and temperatures needs to be determined to estimate the diffusion coefficient of the solutes in the AAIL. The viscosity of the AAIL is strongly affected by the concentration of CO_2-AAIL complexes (com1 and com2). Therefore, the viscosity of the AAIL can be expressed as a function of the concentration of the com1 and com2.

The viscosity of the AAIL under different CO_2 partial pressures was measured to investigate the relationship between the CO_2-AAIL complex concentration and the AAIL viscosity. The concentration of the CO_2-AAIL complexes at certain CO_2 partial pressures and temperatures were calculated using Eqs. 8–13. Figure 2 illustrates the relationship between the mole fraction of the total CO_2-AAIL complex in the AAIL ($x_{\mathrm{com,total}}$) and the AAIL viscosity at 323 K and 373 K. The mole fraction of the total CO_2-AAIL complex ($x_{\mathrm{com,total}}$) is the sum of the mole fractions of com1 (x_{com1}) and com2 (x_{com2}) in the AAIL. As depicted in Figure 2, the viscosity of the AAIL increased with the increase in the mole fraction of the CO_2-AAIL complexes.

The Eqs. 4–6 indicate that unreacted AAIL, com1, com2, and $R\text{-}NH_3^+$ coexist in the AAIL at the equilibrium state of the CO_2 absorption. Consequently, the AAIL after CO_2 absorption could be regarded as a mixture of these components. We used the simple equation (Eq. 17) that expresses the viscosity of the mixture, η_{AAIL} [mPa s], as a linear contribution of the viscosity of each component.[39–41]

$$\eta_{\mathrm{AAIL}} = \eta_{\mathrm{AAIL,neat}} x_{\mathrm{AAIL,neat}} + \eta_{\mathrm{com1}} x_{\mathrm{com1}} + \eta_{\mathrm{com2}} x_{\mathrm{com2}} + \eta_{\mathrm{R-NH3+}} x_{\mathrm{R-NH3+}}, \qquad (17)$$

where, $\eta_{AAIL,neat}$, η_{com1}, η_{com2}, and $\eta_{R\text{-}NH3+}$ [mPa s] are the pure state viscosities of the AAIL, com1, com2, and R–NH_3^+, respectively. x_i [-] is the mole fractions of component i in the AAIL. Since the molar fraction of com2 and R–NH_3^+ are the same, Eq. 17 was rewritten in the following simple formula.

$$\begin{aligned}\eta_{AAIL} &= \eta_{AAIL,neat}x_{AAIL,neat} + \eta_{com1}x_{com1} + (\eta_{com2} + \eta_{R-NH3+})x_{com2} \\ &= \eta_{AAIL,neat}x_{AAIL,neat} + \eta_{com1}x_{com1} + \eta'_{com2}x_{com2},\end{aligned} \quad (18)$$

where η'_{com2} [mPa s] is the sum of η_{com2}, and $\eta_{R–NH3+}$. The mole fraction of each solute of the AAIL at a particular CO_2 partial pressure and temperature could be calculated using Eqs. 8–13. Furthermore, $\eta_{AAIL,neat}$ at both 323 K and 373 K was experimentally measured. Therefore, using η_{com1} and η'_{com2} as the fitting parameters, the relationship between the viscosity of the AAIL and $x_{com,total}$ could be calculated from Eq. 18. As depicted in Figure 2, the calculated results are consistent with the experimental results at both 323 K and 373 K. The determined parameters are listed in Table S1. This result indicated that Eq. 18 was enough accurate to estimate the viscosity of the AAIL after CO_2 absorption.

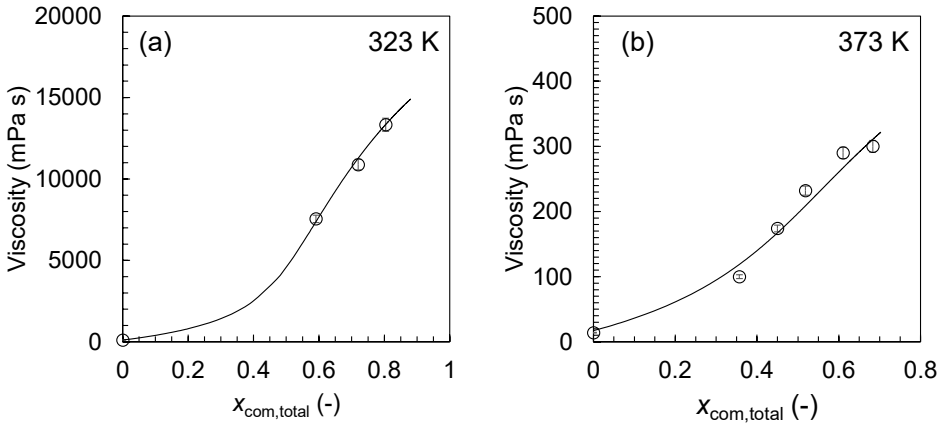

Figure 2 Relationship between the viscosity of [P_{4444}][Gly] and the total mole fraction of the CO_2-AAIL complexes, where $x_{com,total} = x_{com1} + x_{com2}$, at (a)323 K and (b)373 K. The plots and lines indicate the experimental data and the calculated results, respectively.

The temperature dependence of the viscosity needs to be considered to simulate the AAIL viscosity at various CO_2 partial pressures and temperatures. Consequently, the CO_2 partial pressure dependence of the AAIL viscosity was measured at various temperatures. The η_{com1} and η'_{com2} values at each temperature were determined through the aforementioned method. Figure 3(a) illustrates the temperature dependence of the measured $\eta_{AAIL,neat}$ and determined η_{com1} and η'_{com2}. Generally, the temperature dependence of the viscosity of the ionic liquid follows the Vogel–Fulcher–Tammann (VFT) equation.[42,43]

$$\eta_i = A' \exp\left(\frac{B}{T - T_0}\right), \quad (19)$$

where A' [mPa s] and B [K] are empirical constants and T_0 [K] represents the reference temperature. Therefore, temperature dependence of $\eta_{AAIL,neat}$, η_{com1}, and η'_{com2} would follow the VFT equation. The fitting lines for each component are displayed in Figure 3(a). The parameters for the fitting are listed in Table 3. The calculated lines were well fitted to the temperature dependency of the $\eta_{AAIL,neat}$, η_{com1}, and η'_{com2}. Thus, the value of $\eta_{AAIL,neat}$, η_{com1}, and η'_{com2} at any temperature can be calculated from the VFT equation by using the parameters listed in Table 3. This result means that the viscosity of the AAIL at any CO_2 partial pressure and temperature could be estimated through Eq. 18 using the $\eta_{AAIL,neat}$, η_{com1}, and η'_{com2} values determined by the VFT equation.

Figure 3(b) shows the CO_2 partial pressure dependence of the AAIL viscosity measured at various temperatures. The fitted lines illustrated in this figure were estimated through Eq. 18 and the VFT equation. The estimated viscosities are consistent with the experimentally obtained viscosity data. Therefore, our constructed equation estimates the viscosity of the AAIL with high accuracy.

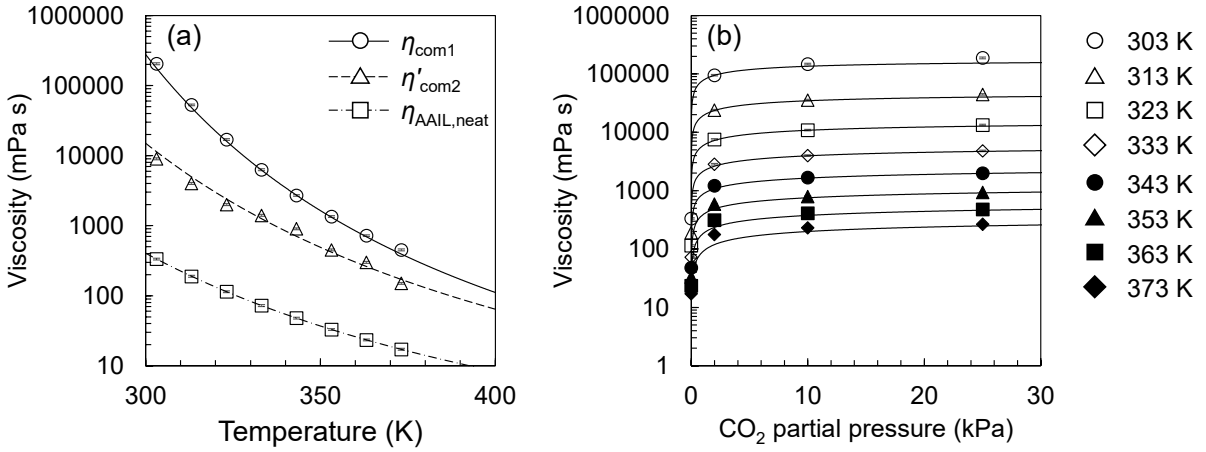

Figure 3 (a) Temperature dependence of $\eta_{AAIL,neat}$, η_{com1}, and η'_{com2}. The lines represent the fitting results from the VFT equation. (b) Relationship between the viscosity of $[P_{4444}][Gly]$ and CO_2 partial pressure at several temperatures. The plots are experimental results and the lines are simulated results obtained using Eq. (18) and (19).

Table 3 Parameters used for fitting based on the VFT equation.

	A' [mPa s]	B [K]	T_0 [K]
$\eta_{AAIL,neat}$	4.40×10^{-4}	1850	129
η_{com1}	7.22×10^{-4}	1900	187
η'_{com2}	7.22×10^{-4}	2100	150

3.3 Estimation of CO_2 permeability of the AAIL-based FTM

3.3.1 Mean viscosity model

The total CO_2 flux can be expressed as the summation of the diffusion fluxes of each solute as shown in Eq. 7. The conventional mean viscosity model approximates the viscosity of the AAIL in the FTM to the constant representative viscosity to simply solve Eq. 7. As the representative viscosity, the average of the viscosities of the AAIL at the feed side membrane surface and the

permeate side membrane surface was adopted. Because the diffusion coefficient has a constant value, the concentration gradient of each solute was considered as constant in the membrane. Therefore, total CO_2 flux through the membrane was expressed using the following simple equation.

$$J_{CO2} = \sum_i \frac{\varepsilon}{\tau} D_{\mathrm{ave,i}} \frac{C_{\mathrm{i,f}} - C_{\mathrm{i,p}}}{l}, \tag{20}$$

where, l [m] is the thickness of the FTM. $C_{\mathrm{i,f}}$ [mol m^{-3}] and $C_{\mathrm{i,p}}$ [mol m^{-3}] are the concentrations of compound i at the feed side surface and permeate side surface, respectively. $D_{\mathrm{ave,i}}$ [m^2 s^{-1}] is the average diffusion coefficient of compound i in the AAIL-based FTM calculated through the mean viscosity using Eq. 16. ε [-] and τ [-] are the porosity and tortuosity of the porous PTFE support, respectively. Additionally, the diffusion controlled CO_2 permeation through the membrane results in the concentrations of the CO_2-AAIL complex near the membrane surface at the feed and permeate sides reaching the absorption equilibrium concentrations of $C_{\mathrm{i,f,eq}}$, [mol m^{-3}] and $C_{\mathrm{i,p,eq}}$ [mol m^{-3}].

3.3.2 Gradient viscosity model

The gradient viscosity model expresses the continuous change of the viscosity of the AAIL in the FTM with dividing the membrane into small intervals as depicted in Figure 4. In this figure, Δz [m] represents the thickness of the intervals when the membrane was divided into n [-] sections. $C_{\mathrm{i,0}}$, $C_{\mathrm{i,1}}$, ⋯, $C_{\mathrm{i,n}}$ are the concentrations of the component i at each boundary of the interval. $D_{\mathrm{i,0}}$, $D_{\mathrm{i,1}}$, ⋯, $D_{\mathrm{i,n}}$ are the diffusion coefficients of component i in the AAIL at each interval. At the steady state, the fluxes of compound i at each interval, $J_{\mathrm{i,1}}$, $J_{\mathrm{i,2}}$, …, $J_{\mathrm{i,n}}$ were assigned the same value (J_{i}) after considering the mass balance. When the rate determining step of the FTM is the

diffusion process, J_i in each interval are determined by the diffusion flux of compound i. Moreover, the diffusion-controlled CO_2 permeation suggests the boundary conditions that $C_{i,0}$ and $C_{i,n}$ are equal to $C_{i,f,eq}$, and $C_{i,p,eq}$, respectively. Therefore, the following equations describe J_i that hold for each interval as follows.

$$J_i = \frac{\varepsilon}{\tau} D_{i,1} \frac{C_{i,f} - C_{i,1}}{\Delta z} \tag{21-1}$$

$$J_i = \frac{\varepsilon}{\tau} D_{i,2} \frac{C_{i,1} - C_{i,2}}{\Delta z} \tag{21-2}$$

$$\vdots$$

$$J_i = \frac{\varepsilon}{\tau} D_{i,n} \frac{C_{i,n-1} - C_{i,n}}{\Delta z} \tag{21-3}$$

From the Eq. 21, the following relationship between $C_{i,k}$ and $C_{i,k+1}$ is obtained.

$$C_{i,k+1} = C_{i,k} - \frac{J_i \Delta z}{\frac{\varepsilon}{\tau} D_{i,k}}, \tag{22}$$

where $C_{i,k}$ and $C_{i,k+1}$ are the concentration of component i at the boundary of the interval k and k + 1, respectively.

On the other hand, for the liquid-based FTM, the diffusion coefficient of each component in the AAIL at interval k, $D_{i,k}$, could be calculated using the Wilke-Chang equation using the viscosity of the AAIL at the interval k, $\eta_{AAIL,k}$. Here, $\eta_{AAIL,k}$ can be estimated by Eq. 18 using the mole fraction of each component at the feed side boundary of the interval k, $x_{i,k}$, that was determined by the $C_{i,k}$. Consequently, $C_{i,k+1}$ can be calculated from Eq. 22 using the $C_{i,k}$ and J_i. The $C_{i,f,eq}$ can be determined at a particular CO_2 partial pressure and temperature through Eqs. 8–13. Therefore, applying the boundary conditions, $C_{i,0} = C_{i,f,eq}$, the values of $C_{i,1}$, $C_{i,2}$, …, $C_{i,n}$ were calculated by sequentially solving Eq. 22 using the arbitrarily set J_i value. The J_i value satisfying

the boundary condition of $C_{i,n} = 0$ (permeate side surface) was determined using a trial and error method. Subsequently, the total CO_2 flux, J_{CO2}, was determined by adding each value of J_i.

This model can be used to the liquid-based FTMs when its rate-determining step is the diffusion process.

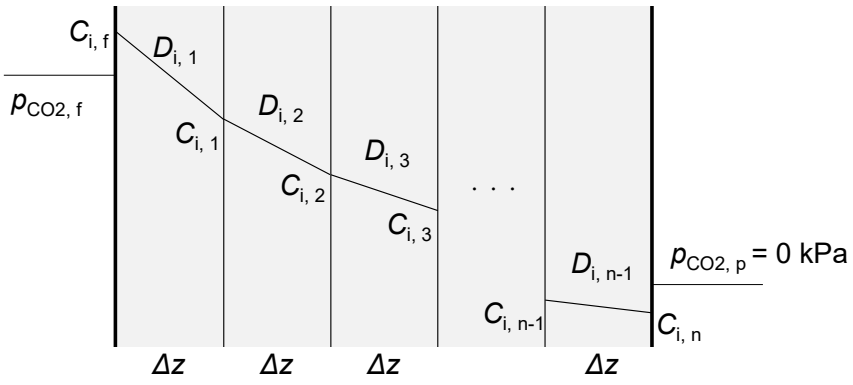

Figure 4 Schematic of the gradient viscosity model.

3.3.3 Validity of the two estimation models

The validity of the mean viscosity model and the gradient viscosity model was investigated by estimating the CO_2 partial pressure dependence of the CO_2 permeabilities of the AAIL-based FTM at 323 K and 373 K. The parameters used for the estimation of this relationship are listed in Table 4. For the gradient viscosity model, the division number, n, was set to 5000 (supporting information). In the calculation, com1 and com2 have the same molar volume value of 403.7 cm^3 mol^{-1} since the chemical structures of these compounds are nearly the same. The molar volume at certain temperature was calculated from the molecular weight of the $[P_{4444}][Gly\text{-}CO_2]$ complex and the density of the AAIL at the temperature (supporting information). Consequently, the same value for D_{com}, was used as D_{com1} and D_{com2} in both the mean viscosity model and the gradient viscosity model.

Figure 5 demonstrates the estimated results of the mean viscosity model (dotted line) and gradient viscosity model (solid line) along with the experimental data. The experimental data obtained in this study was well correlated with the previously reported results.[38] Figure 5(a) clearly indicates that the CO_2 partial pressure dependency of the CO_2 permeability estimated by the gradient viscosity model is consistent with the experimental data at both temperatures. The temperature dependency of the CO_2 permeability estimated by the model was also consistent with the experimental data at each CO_2 partial pressure, as illustrated in Figure 5(b). The difference between the experimental results and the results calculated by the gradient viscosity model were quantified by the relative error of the calculated result to the experimental results at 313.15 K and 373.15 K for each CO_2 partial pressure of 2.5 kPa and 10 kPa. For the CO_2 partial pressure of 2.5 kPa, the relative errors were 20.9 % and 4.18 % at 313.15 K and 373.15 K, respectively. On the other hand, for the CO_2 partial pressure of 10 kPa, the relative errors were 8.63 % and 8.40 % at 313.15 K and 373.15 K, respectively.

Conversely, the values estimated from the mean viscosity model does not correspond well with the experimental data. Moreover, the difference between the estimated values and the experimental values increase with the decrease of temperature. The difference between the experimental results and the results calculated by the mean viscosity model were also quantified by the relative error of the calculated result to the experimental results. For the CO_2 partial pressure of 2.5 kPa, the relative errors were 73.3 % and 28.9 % at 313.15 K and 373.15 K, respectively. On the other hand, for the CO_2 partial pressure of 10 kPa, the relative errors were 47.4 % and 31.3 % at 313.15 K and 373.15 K, respectively.

Table 4 Parameters used for the estimation of the CO_2 permeabilities of the [P_{4444}][Gly]-based FTM.

Parameters	Dimension	Value	Ref
ψ_{AAIL}	[-]	2	[38]
M_{AAIL}	[g mol^{-1}]	333.49	-
V_{CO_2}	[cm^3 mol^{-1}]	34	[33]
ε	[-]	0.5	[38]
τ	[-]	1.2	[38]
l	[m]	3.5×10^{-5}	-
Division number, n	[-]	5000	-

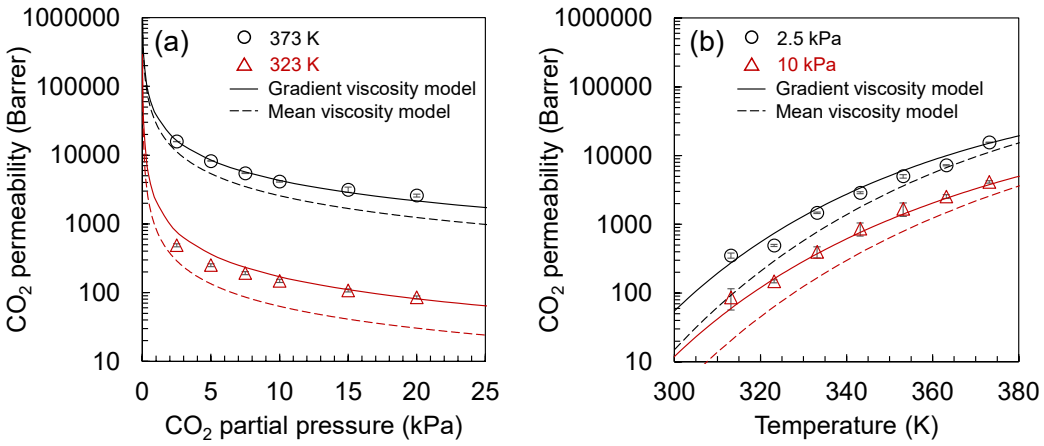

Figure 5 Comparison of the experimental and calculated CO_2 permeability of the supported [P_{4444}][Gly] membrane simulated using the two models against (a)CO_2 partial pressure and (b)temperature. The error bars in both figures are standard deviation of each data.

The poor estimation of the CO_2 permeability using the mean viscosity model was primarily due to its assumption that the D_{com} inside the membrane was constant. Figure 6(a) displays the concentration distribution of the com1 and com2, and the D_{com} change in the AAIL-based FTM

calculated using the gradient viscosity model. As shown in Figure 6(a), the D_{com} changes drastically with the change of the concentration of the CO_2-AAIL complex at each position in the FTM. The D_{com} value at the feed side was low because of the high concentrations of com1 and com2. On the other hand, as the complexes diffuse in the membrane, the concentration of the complexes became lower. So that, the D_{com} value in the membrane was gradually increased.

Figure 6(b) displays the D_{com} at each position of the membrane at 323 K and 373 K calculated by using the gradient viscosity model. The D_{com} at 323 K changed dynamically in the FTM as compared to the value obtained at 373 K. This is because the viscosity difference between the complexes (com1 and com2) and the neat AAIL at low temperature was greater than that at high temperature (Figure 3(a)). The viscosity increase of the AAIL after CO_2 absorption is a consequence of the hydrogen-bonded network formed between the complexes. The hydrogen bond formed in the AAIL would be broken by heating. Therefore, the viscosity increase of the AAIL after CO_2 absorption was not as severe at high temperatures. Since the continuous changes of the D_{com} in the FTM at low temperatures was large, it was difficult for the mean viscosity model to estimate the CO_2 permeability of the AAIL-based FTM accurately. Thus, the mean viscosity model cannot be used for the estimation of the CO_2 permeability at low temperature. Conclusively, the CO_2 permeability of the AAIL-based FTMs having large viscosity changes can be estimated accurately using the gradient viscosity model.

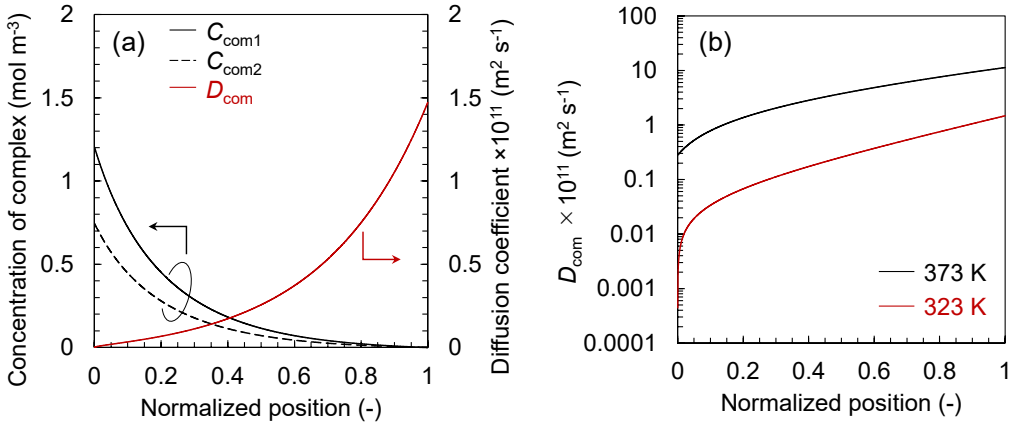

Figure 6 (a) Normalized membrane position dependence of the diffusion coefficient of complexes and the concentration of com1 and com2 at T = 323 K and p_{CO_2} = 10 kPa. (b) Relationship between normalized membrane position and diffusion coefficient of the complexes at 323 K and 373 K. In both figures, the normalized position of "0" and "1" indicates the feed-side membrane surface and permeate-side membrane surface, respectively.

4. CONCLUSION

Herein, a model for estimating the CO_2 permeability of the [P_{4444}][Gly] containing FTM was investigated. We considered two models, namely the mean viscosity model, and the gradient viscosity model and explored the effect of the viscosity gradient of the AAIL inside the FTM on the CO_2 permeability. The mean viscosity model approximated the viscosity of the AAIL in the FTM using a constant representative viscosity and the gradient viscosity model used a viscosity gradient of the AAIL in the FTM by dividing the membrane into small intervals. The CO_2 permeability of the AAIL-based FTM was estimated using these two models and compared to experimental results obtained from literature.

The CO_2 permeability estimated using the mean viscosity model was not consistent with the experimental data. The substantial change of the diffusion coefficient inside the FTM could

explain the poor estimation of the CO_2 permeability using the mean viscosity model. Conversely, the estimated results using the gradient viscosity model was consistent with the experimental data at every CO_2 partial pressure and temperature. Therefore, the viscosity gradient model is effective in estimating the CO_2 permeability of FTMs having a diffusion medium with variable viscosities at different positions in the membrane.

Supporting Information.

The following files are available free of charge. The detail synthesis procedure of $[P_{4444}][Gly]$, experimental set up for gas permeation test, temperature dependency of density of $[P_{4444}][Gly]$, values of η_{com1} and η'_{com2} at several temperatures determined by the fitting, and effect of division number on the calculation of the gradient viscosity model (docx).

REFERENCES

[1] R.W. Baker, K. Lokhandwala, Natural gas processing with membranes: An overview, Ind. Eng. Chem. Res. 47 (2008) 2109–2121.

[2] P. Bernardo, E. Drioli, G. Golemme, Membrane gas separation: A review/state of the art, Ind. Eng. Chem. Res. 48 (2009) 4638–4663.

[3] S. Basu, A.L. Khan, A. Cano-Odena, C. Liu, I.F.J. Vankelecom, Membrane-based technologies for biogas separations, Chem. Soc. Rev. 39 (2010) 750–768.

[4] L.M. Robeson, The upper bound revisited, J. Memb. Sci. 320 (2008) 390–400.

[5] Y. Li, S. Wang, G. He, H. Wu, F. Pan, Z. Jiang, Facilitated transport of small molecules and ions for energy-efficient membranes, Chem. Soc. Rev. 44 (2015) 103–118.

[6] R. Yegani, H. Hirozawa, M. Teramoto, H. Himei, O. Okada, T. Takigawa, N. Ohmura, N. Matsumiya, H. Matsuyama, Selective separation of CO_2 by using novel facilitated transport membrane at elevated temperatures and pressures, J. Memb. Sci. 291 (2007) 157–164.

[7] Y. Han, W.S. Winston Ho, Recent advances in polymeric facilitated transport membranes for carbon dioxide separation and hydrogen purification, J. Polym. Sci. 58 (2020) 2435–2449.

[8] E. Tsuchida, H. Nishide, M. Ohyanagi, H. Kawakami, P. Chemistry, R. October, Facilitated Transport of Molecular Oxygen in the Membranes of Polymer-Coordinated Cobalt Schiff Base Complexes, Macromolecules. 20 (1987) 1907–1912.

[9] H.S. Kim, H. Kim, B.S. Ahn, J.H. Ryu, Y.S. Kang, Reversible olefin complexation by silver ions in dry poly(vinyl methyl ketone) membrane and its application to olefin/paraffin separations, Chem. Commun. (2000) 1261–1262.

[10] Y.Y. Lee, B. Gurkan, Graphene oxide reinforced facilitated transport membrane with poly(ionic liquid) and ionic liquid carriers for CO_2/N_2 separation, J. Memb. Sci. 638 (2021) 119652.

[11] Z. Zhang, S. Rao, Y. Han, R. Pang, W.S.W. Ho, CO_2-selective membranes containing amino acid salts for CO_2/N_2 separation, J. Memb. Sci. 638 (2021) 119696.

[12] Z. Tu, P. Liu, X. Zhang, M. Shi, Z. Zhang, S. Luo, L. Zhang, Y. Wu, X. Hu, Highly-selective separation of CO_2 from N_2 or CH_4 in task-specific ionic liquid membranes: Facilitated transport and salting-out effect, Sep. Purif. Technol. 254 (2021) 117621.

[13] S. Janakiram, J.L. Martín Espejo, X. Yu, L. Ansaloni, L. Deng, Facilitated transport membranes containing graphene oxide-based nanoplatelets for CO_2 separation: Effect of 2D filler properties, J. Memb. Sci. 616 (2020) 118626.

[14] T.E. Rufford, S. Smart, G.C.Y. Watson, B.F. Graham, J. Boxall, J.C. Diniz da Costa, E.F. May, The removal of CO_2 and N_2 from natural gas: A review of conventional and emerging process technologies, J. Pet. Sci. Eng. 94–95 (2012) 123–154.

[15] U.W.R. Siagian, A. Raksajati, N.F. Himma, K. Khoiruddin, I.G. Wenten, Membrane-based carbon capture technologies: Membrane gas separation vs. membrane contactor, J. Nat. Gas Sci. Eng. 67 (2019) 172–195.

[16] J. Huang, J. Zou, W.S.W. Ho, Carbon dioxide capture using a CO_2-selective facilitated transport membrane, Ind. Eng. Chem. Res. 47 (2008) 1261–1267.

[17] M.K. Mondal, H.K. Balsora, P. Varshney, Progress and trends in CO_2 capture/separation technologies: A review, Energy. 46 (2012) 431–441.

[18] N. Matsumiya, M. Teramoto, S. Kitada, H. Matsuyama, Evaluation of energy consumption for separation of CO_2 in flue gas by hollow fiber facilitated transport membrane module with permeation of amine solution, Sep. Purif. Technol. 46 (2005) 26–32.

[19] M. Saeed, S. Rafiq, L.H. Bergersen, L. Deng, Tailoring of water swollen PVA membrane for hosting carriers in CO_2 facilitated transport membranes, Sep. Purif. Technol. 179 (2017) 550–560.

[20] S. Kasahara, E. Kamio, T. Ishigami, H. Matsuyama, Amino acid ionic liquid-based facilitated transport membranes for CO_2 separation, Chem. Commun. 48 (2012) 6903–6905.

[21] S. Kasahara, E. Kamio, A.R. Shaikh, T. Matsuki, H. Matsuyama, Effect of the amino-group densities of functionalized ionic liquids on the facilitated transport properties for CO_2 separation, J. Memb. Sci. 503 (2016) 148–157.

[22] S. Kasahara, E. Kamio, H. Matsuyama, Improvements in the CO_2 permeation selectivities of amino acid ionic liquid-based facilitated transport membranes by controlling their gas absorption properties, J. Memb. Sci. 454 (2014) 155–162.

[23] F. Moghadam, E. Kamio, T. Yoshioka, H. Matsuyama, New approach for the fabrication of double-network ion-gel membranes with high CO_2/N_2 separation performance based on facilitated transport, J. Memb. Sci. 530 (2017) 166–175.

[24] F. Moghadam, E. Kamio, A. Yoshizumi, H. Matsuyama, An amino acid ionic liquid-based tough ion gel membrane for CO_2 capture, Chem. Commun. 51 (2015) 13658–13661.

[25] F. Moghadam, E. Kamio, H. Matsuyama, High CO_2 separation performance of amino acid ionic liquid-based double network ion gel membranes in low CO_2 concentration gas mixtures under humid conditions, J. Memb. Sci. 525 (2017) 290–297.

[26] A.G. Ogston, The spaces in a uniform random suspension of fibres, Trans. Faraday Soc. 54 (1958) 1754–1757.

[27] B.F. Goodrich, J.C. De La Fuente, B.E. Gurkan, Z.K. Lopez, E.A. Price, Y. Huang, J.F. Brennecke, Effect of water and temperature on absorption of CO_2 by amine-functionalized anion-tethered ionic liquids, J. Phys. Chem. B. 115 (2011) 9140–9150.

[28] X. Wang, N.G. Akhmedov, Y. Duan, D. Luebke, D. Hopkinson, B. Li, Amino acid-functionalized ionic liquid solid sorbents for post-combustion carbon capture, ACS Appl. Mater. Interfaces. 5 (2013) 8670–8677.

[29] J.L. McDonald, R.E. Sykora, P. Hixon, A. Mirjafari, J.H. Davis, Impact of water on CO_2 capture by amino acid ionic liquids, Environ. Chem. Lett. 12 (2014) 201–208.

[30] M.S. Raja Shahrom, C.D. Wilfred, D.R. MacFarlane, R. Vijayraghavan, F.K. Chong, Amino acid based poly(ionic liquid) materials for CO_2 capture: Effect of anion, J. Mol. Liq. 276 (2019) 644–652.

[31] D. Morgan, L. Ferguson, P. Scovazzo, Diffusivities of gases in room-temperature ionic Liquids: Data and correlations obtained using a lag-time technique, Ind. Eng. Chem. Res. 44 (2005) 4815–4823.

[32] J.H. Arnold, Studies in diffusion. II. A kinetic theory of diffusion in liquid systems, J. Am. Chem. Soc. 52 (1930) 3937–3955.

[33] C.R. Wilke, P. Chang, Correlation of Diffusion Coefficients in Dilute Solutions, Aiche J. 1 (1955) 264–270.

[34] R. Rea, M.G. De Angelis, M.G. Baschetti, Models for facilitated transport membranes: A review, Membranes. 9 (2019).

[35] M. Teramoto, K. Nakai, N. Ohnishi, Q. Huang, T. Watari, H. Matsuyama, Facilitated Transport of Carbon Dioxide through Supported Liquid Membranes of Aqueous Amine Solutions, Ind. Eng. Chem. Res. 35 (1996) 538–545.

[36] M. Teramoto, Q. Huang, T. Watari, Y. Tokunaga, R. Nakatani, T. Maeda, H. Matsuyama, Facilitated transport of CO_2 through supported liquid membranes of various amine solutions - Effects of rate and equilibrium of reaction between CO_2 and amine-, J. Chem. Eng. Japan. 30 (1997) 328–335.

[37] M. Teramoto, N. Takeuchi, T. Maki, H. Matsuyama, Facilitated transport of CO_2 through liquid membrane accompanied by permeation of carrier solution, Sep. Purif. Technol. 27 (2002) 25–31.

[38] S. Kasahara, E. Kamio, A. Otani, H. Matsuyama, Fundamental investigation of the factors controlling the CO_2 permeability of facilitated transport membranes containing amine-functionalized task-specific ionic liquids, Ind. Eng. Chem. Res. 53 (2014) 2422–2431.

[39] E. Gómez, B. González, Á. Domínguez, E. Tojo, J. Tojo, Dynamic viscosities of a series of 1-alkyl-3-methylimidazolium chloride ionic liquids and their binary mixtures with water at several temperatures, J. Chem. Eng. Data. 51 (2006) 696–701.

[40] P. Navia, J. Troncoso, L. Romaní, Viscosities for ionic liquid binary mixtures with a common ion, J. Solution Chem. 37 (2008) 677–688.

[41] D.E. Goldsack, A.A. Franchetto, The viscosity of concentrated electrolyte solutions-III. A mixture law, Electrochim. Acta. 22 (1977) 1287–1294.

[42] K.R. Harris, M. Kanakubo, L.W. A., Temperature and Pressure Dependence of the Viscosity of the Ionic Liquid 1-Butyl-3-methylimidazolium Acetate, J. Chem. Eng. Data. 65 (2020) 804–813.

[43] Y. Wei, Y. Jin, Z.J. Wu, Y. Yang, Q.G. Zhang, Z.H. Kang, Synthesis and physicochemical properties of amino acid ionic liquid 1-butyl-3-methylimidazolium aspartate and binary mixture with methanol, J. Chem. Eng. Data. 58 (2013) 349–356.

Supporting Information

A gradient viscosity model for estimating CO_2 permeability of amino acid ionic liquid-based facilitated transport membrane

Atsushi Matsuoka, Akihito Otani, Eiji Kamio, and Hideto Matsuyama[*]

Research Center for Membrane and Film Technology, Department of Chemical Science and Engineering, Kobe University, 1-1 Rokkodai, Nada, Kobe 657-8501, Japan

[*]Corresponding author.
E-mail address: matuyama@kobe-u.ac.jp

Contents:

1. Synthesis of $[P_{4444}][Gly]$
2. Experimental setup for gas permeation test
3. Density measurement of $[P_{4444}][Gly]$
4. Value of η_{com1} and η'_{com2} at several temperatures determined by the fitting
5. Effect of division number on the calculation of the gradient viscosity model
6. TG-DTA analysis of the $[P_{4444}][Gly]$
7. Long time stability of the SILM with $[P_{4444}][Gly]$
8. Molar fraction of com1 and com2 in the CO_2 absorbed AAIL
9. Time course of the viscosity of $[P_{4444}][Gly]$ during the CO_2 absorption
10. Comparison of the gas permeation performance

S1. *Synthesis of [P_{4444}][Gly]*

[P_{4444}][Gly]

The neutralization reaction between tetrabutylphosphonium hydroxide ([P_{4444}][OH]) 40 wt% in H_2O (100 g) and L-glycine (10.8 g) was carried out for 12 h at 298 K. After the reaction, the water was removed by evaporation at 333 K for 6 h. Then the mixture of methanol/acetonitrile = 1/9 v/v was added to the residue. After 30 min stirring, the precipitated unreacted L-glycine was removed by filtration. The solvent was removed by evaporation at 313 K for 6 h. Obtained liquid was dried in vacuo at 373 K for 24 h.

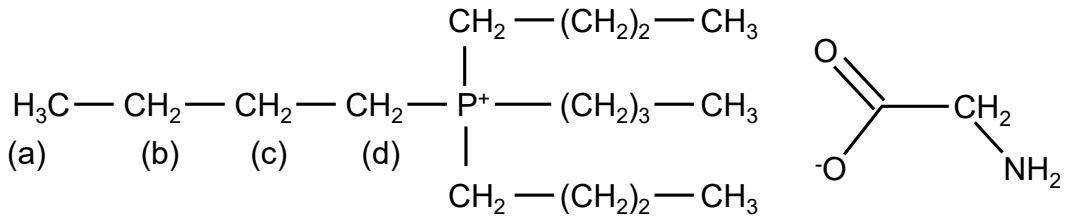

^{1}H-NMR (DMSO, σ/ppm relative to TMS)

σ = 0.92 (t, 12H, J = 7.1; a), 1.37-1.50 (m, 16H; b,c), 2.16-2.22 (m, 8H; d), 2.64 (s, 2H; N-CH_2-CO_2)

S2. *Experimental setup for gas permeation test*

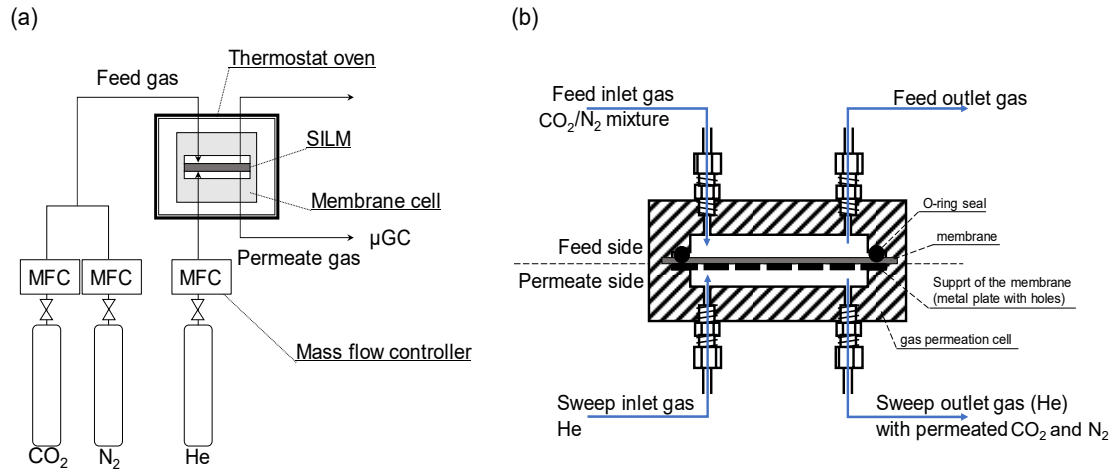

Figure S1 Schematic image of the (a) apparatus and (b) membrane cell used for the gas permeation test.

S3. *Density measurement of [P_{4444}][Gly]*

Density of [P_{4444}][Gly] was measured by a density/specific gravity meter (DA-650, Kyoto Electronics Manufacturing Co., Ltd., Kyoto, Japan). The densities were measured at temperatures in the range of 303–363 K. Fig. S2 shows the temperature dependency of the density of the AAIL. The density of the AAIL was linearly decreased with the increase of the temperature. Density of the AAIL at 373 K was estimated from the fitting curve in the Fig. S2.

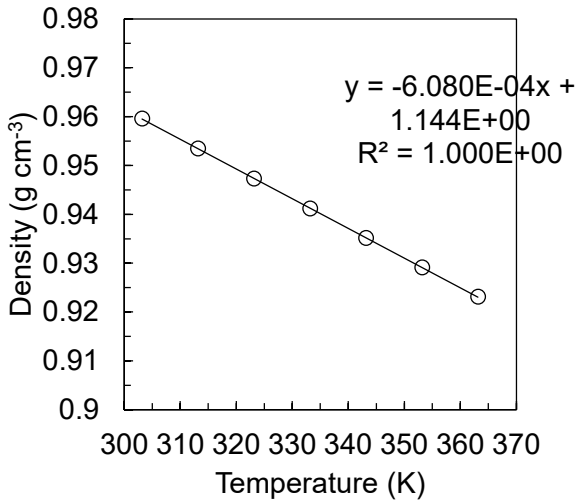

Figure S2 Temperature dependency of the density of [P_{4444}][Gly]. Plots are the experimental result and line is fitting curve.

S4. *Values of $\eta_{AAIL,neat}$, η_{com1} and η'_{com2} at several temperatures determined by the fitting*

Table S1 *$\eta_{AAIL,neat}$, η_{com1} and η'_{com2}* at several temperatures.

Temperature [K]	$\eta_{AAIL,neat}$ [mPa s]	η_{com1} [mPa s]	η'_{com2} [mPa s]
303.15	334.0	205000	9000
313.15	189.5	53000	4000
323.15	114.2	17000	2000
333.15	72,4	6300	1400
343.15	47.9	2700	900
353.15	32.9	1350	450
363.15	23.4	720	300
373.15	17.1	450	150

S5. *Effect of division number on the calculation of the gradient viscosity model*

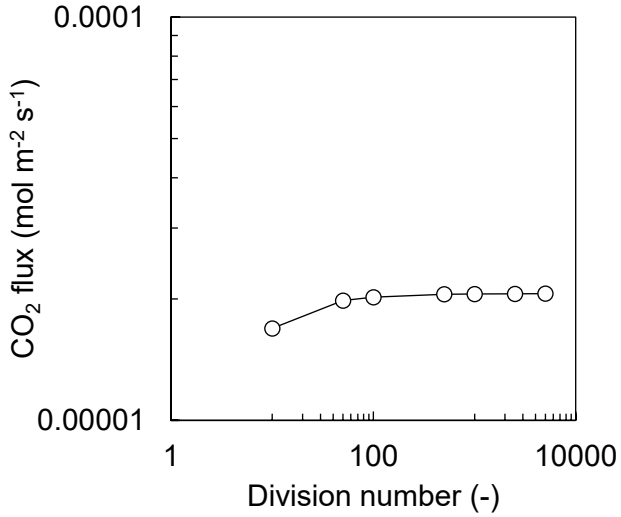

Figure S3 Relationship between the division number and the calculated CO_2 flux by the gradient viscosity model. p_{CO2} = 1 kPa, T = 323.15 K

S6. *TG-DTA analysis of the [P_{4444}][Gly]*

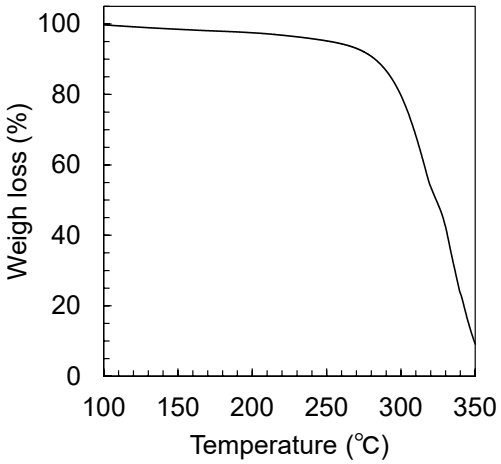

Figure S4 TGA profiles of [P_{4444}][Gly] under N_2 using temperature ramp rate of 10 K/min.

S7. *Long time stability of the SILM with [P_{4444}][Gly]*

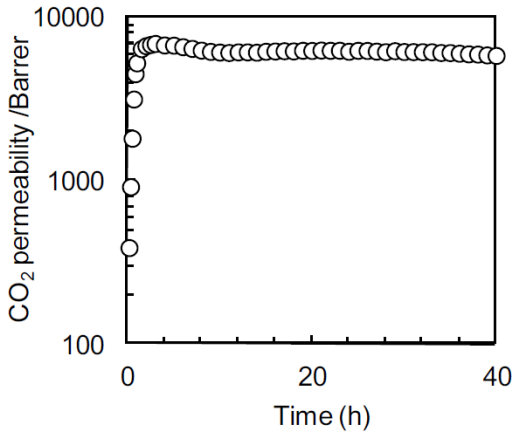

Figure S5 Time course of CO_2 permeability through the SILM with [P_{4444}][Gly]. (T = 373.15 K, p_{CO2} = 10 kPa)

S8. *Molar fraction of com1 and com2 in the CO_2 absorbed AAIL*

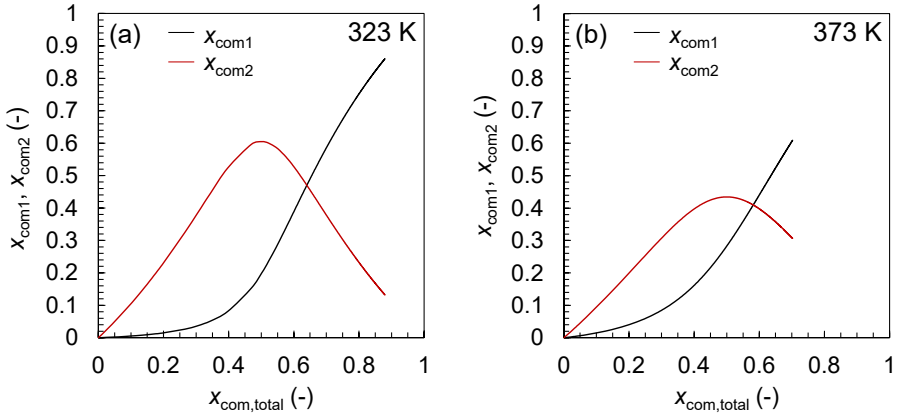

Figure S6 Relationship between the molar fraction of com1 and com2 in the AAIL, x_{com1} and x_{com2}, and the total CO_2 absorption amount, $x_{com,total}$, at (a)323 K and (b)373 K.

S9. *Time course of the viscosity of [P_{4444}][Gly] during the CO_2 absorption*

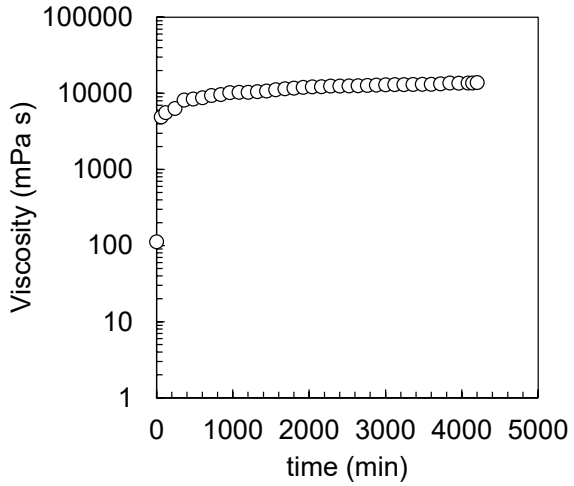

Figure S7 Time course of the viscosity of [P_{4444}][Gly] during the CO_2 absorption. (T = 323.15 K, p_{CO2} = 25 kPa)

S10. *Comparison of the gas permeation performance*

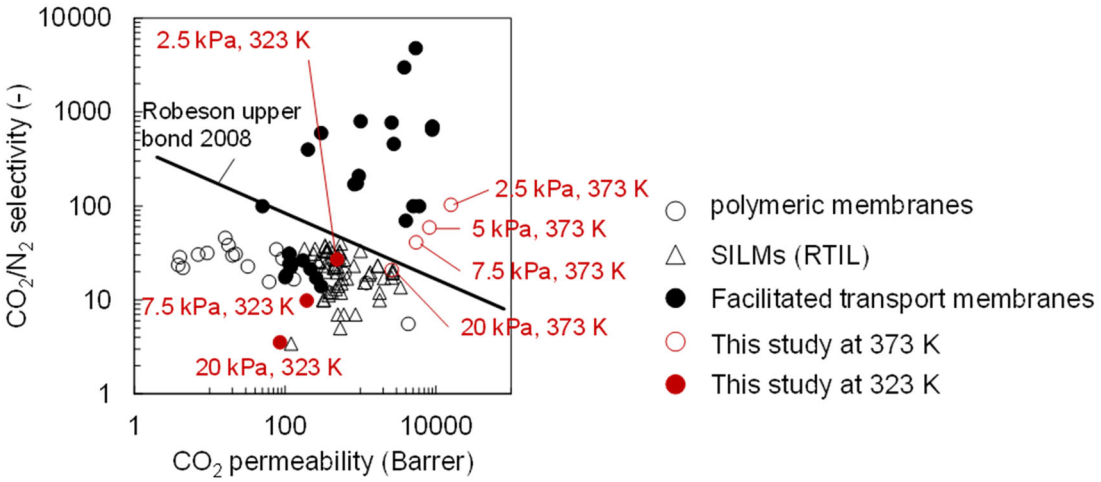

Figure S8 Robeson's plot of the reported polymeric membranes, SILMs with room temperature ionic liquid, FTMs, and AAIL-based FTMs used in this study.

References

1. Bara, Jason E.; Hatakeyama, Evan S.; Gabriel, Christopher J.; Zeng, Xiaohui; Lessmann, Sonja; Gin, Douglas L.; Noble, Richard D.,Synthesis and light gas separations in cross-linked gemini room temperature ionic liquid polymer membranes, Journal of Membrane Science, 316, 186-191, 2008
2. Bara, Jason E.; Lessmann, Sonja; Gabriel, Christopher J.; Hatakeyama, Evan S.; Noble, Richard D.; Gin, Douglas L., Synthesis and Performance of Polymerizable Room-Temperature Ionic Liquids as Gas Separation Membranes, Industrial & Engineering Chemistry Research, 46, 5397-5404, 2007
3. Sakaguchi, Toshikazu; Takeda, Aiko; Hashimoto, Tamotsu, Highly Gas-Permeable Silanol-Functionalized Poly(diphenylacetylene)s: Synthesis, Characterization, and Gas Permeation Property, Macromolecules, 44, 6810-6817, 2011
4. Wolinska-Grabczyk, Aleksandra; Jankowski, Andrzej, CO_2/N_2 separation ability and structural characteristics of poly(butadiene-co-acrylonitrile)-based polyurethanes and hydrogenated nitrile rubbers, Journal of Applied Polymer, Science, 122, 2690-2696, 2011
5. Close, Joshua J.; Farmer, Karen; Moganty, Surya S.; Baltus, Ruth E., CO_2/N_2 separations using nanoporous alumina-supported ionic liquid membranes: Effect of the support on separation performance, Journal of Membrane Science, 390, 201-210, 2012
6. Carlisle, Trevor K.; Nicodemus, Garret D.; Gin, Douglas L.; Noble, Richard D., CO_2/light gas separation performance of cross-linked poly(vinylimidazolium) gel membranes as a function of ionic liquid loading and cross-linker content, Journal of Membrane Science, 397, 24-37, 2012

7. Mahurin, Shannon M.; Dai, Thomas; Yeary, Joshua S.; Luo, Huimin; Dai, Sheng, Benzyl-Functionalized Room Temperature Ionic Liquids for CO_2/N_2 Separation, Industrial & Engineering Chemistry Research, 50, 14061-14069, 2011
8. Zhien Zhang, Shraavya Rao, Yang Han, Ruizhi Pang, W.S. Winston Ho, CO_2-selective membranes containing amino acid salts for CO_2/N_2 separation, Journal of Membrane Science, 638, 119696, 2021
9. Kovvali, A. Sarma; Chen, Hua; Sirkar, Kamalesh K., Dendrimer Membranes: A CO_2-Selective Molecular Gate, Journal of the American Chemical Society, 122, 7594-7595, 2000
10. Ji, Pengfei; Cao, Yiming; Zhao, Hongyong; Kang, Guodong; Jie, Xingming; Liu, Dandan; Liu, Jianhui; Yuan, Quan, Preparation of hollow fiber poly(N,N-dimethylaminoethyl methacrylate)-poly(ethylene glycol methyl ether methyl acrylate)/polysulfone composite membranes for CO_2/N_2 separation, Journal of Membrane Science, 342, 190-197, 2009